Active Vibration Control with Model Correction on a Flexible Laboratory Grid Structure

George C. Schamel II* and Raphael T. Haftka†
Virginia Polytechnic Institute and State University, Blacksburg, Virginia 24061

This paper presents experimental and computational comparisons of three active damping control laws applied to a complex laboratory structure. Two reduced structural models were used with one model being corrected on the basis of measured mode shapes and frequencies. Three control laws were investigated, a time-invariant linear quadratic regulator with state estimation and two direct rate feedback control laws. Experimental results for all designs were obtained with digital implementation. It was found that model correction improved the agreement between analytical and experimental results. The best agreement was obtained with the simplest direct rate feedback control.

Nomenclature

c = inherent damping matrix
D = active damping matrix, $n_c \times n_c$
e = state reconstruction error vector, $2n \times 1$
F_D = gain matrix, $n_c \times 2n$
f_i = maximum force ratio or performance index
g_j = jth constraint in optimization problems
I = identity matrix of appropriate order
k = structural stiffness matrix
M_i = ith modal mass, $i = 1, \ldots, n_R$
m = mass matrix
n = number of degrees of freedom
n_c = number of control actuators
n_f = number of initial conditions
n_m = number of stability margin constraints
n_R = number of degrees of freedom of reduced model
n_s = number of sensors
q = vector of physical displacements, $n \times 1$
$\dot{q}_j$ = velocity measured by jth sensor, $j = 1, \ldots, n_s$
S = Riccati solution matrix for regulator design
U = applied load distribution matrix, $n \times n_c$
u = control input vector, $n_c \times 1$
V_1 = system noise matrix
V_2 = measurement noise matrix
w_1 = vector of state excitation noise, $2n \times 1$
x = state vector of structural motion, $2n \times 1$
y = sensor output vector
β = performance index
ζ = damping ratio
Φ = modal matrix, $n \times n$
ϕ_i = open-loop modal vector of mode i
ω_i = ith natural frequency
0 = zero matrix of appropriate order

Subscripts

E = augmented reconstructed matrix
L = lower limit
R = reduced model
0 = initial value

Superscripts

$\hat{}$ = corrected reduced system
$-$ = augmented system
$\sim$ = closed-loop system
$'$ = estimated state

Introduction

CURRENTLY, there is great interest in the active vibration control of large space structures (e.g., Refs. 1-14). Many analytical studies are based on a linear quadratic (LQ) optimal control. This control strategy requires a controller of the same order as the model of the structure. A finite element model of the structure is usually of high order so that an LQ control system based on that model would be difficult to design and practically impossible to implement. Consequently, the control system is designed based on a reduced-order model including the first few vibration modes and a limited number of degrees of freedom. This modal truncation of the structural model can result in a control system that destabilizes higher-order modes, a phenomenon known as spillover instability.[1] For this reason, there is interest in modifying the LQ design process to guarantee the stability of the unmodeled dynamics (e.g., Ref. 2).

Even with a reduced-order model of the structure, the LQ system design may be difficult to implement. For this reason, many experimental studies simulating the control of large space structures have employed simple control laws.[3-7] Reference 3 proposed two simple direct rate feedback (DRF) control laws for active damping that guaranteed system stability[4] and approached or bettered the performance of the LQ regulator with state estimation. One control law is based on the same quadratic performance index as LQ control and the other is designed to minimize the maximum control force. The authors of Ref. 3 applied the control laws to a relatively simple beam structure. The objective of the present paper is to apply the DRF control laws to a more complex structure that requires the use of system identification techniques to improve the structural model.

Equations of Motion

The equations of motion for a structure with n degrees of freedom (DOF) and controlled by n_c actuators are

$$m\ddot{q}(t) + c\dot{q}(t) + kq(t) = Uu(t) \tag{1}$$

where m, c, and k are the mass, inherent viscous damping, and stiffness matrices, respectively. We assume that c does not couple the normal modes of vibration (i.e., proportional

Received Aug. 2, 1989; revision received Sept. 23, 1990; accepted for publication Sept. 23, 1990.

*Graduate Research Assistant, Department of Aerospace Engineering; current address, 11162 Conifer Mountain Road, Conifer, CO 80433. Member AIAA.

†Christopher Kraft Professor, Department of Aerospace Engineering. Member AIAA.

damping). U is an applied load distribution matrix relating the control input vector u to the structural DOF, and q is a vector of physical or generalized displacement components. We assume these matrices are constant.

Including uncertainties and random excitation in the form of a vector $w_1(t)$, the equations of motion are written for the state vector $x = [\dot{q}^T, q^T]^T$ as

$$\dot{x}(t) = A\,x(t) + B\,u(t) + w_1(t) \tag{2}$$

with

$$A = \begin{bmatrix} -m^{-1}c & -m^{-1}k \\ I & 0 \end{bmatrix}, \qquad B = \begin{bmatrix} m^{-1}U \\ 0 \end{bmatrix} \tag{3}$$

Model Reduction Methods

The order of the analytical model may have to be reduced from n to n_R to meet the physical limitations of the control hardware. Two model reduction techniques are used in this paper that retain physical degrees of freedom (rather than modal amplitudes) as generalized coordinates. The first method preserves exactly the first n_R normal modes and frequencies of the original model.[9] The reduced-order state vector q_R does not consist of modal amplitudes, but of a subset of n_R degrees of freedom in q. The reduced matrices needed for obtaining reduced system and control matrices A_R and B_R are given as

$$m_R^{-1}\,c_R = \Phi_R[\mathrm{diag}(2\zeta_i\omega_i)]_R\,\Phi_R^{-1} \tag{4}$$

$$m_R^{-1}\,k_R = \Phi_R[\mathrm{diag}(\omega_i^2)]_R\,\Phi_R^{-1} \tag{5}$$

$$m_R^{-1}\,U_R = \Phi_R[\mathrm{diag}(M_i^{-1})]_R\,\Phi_R^T\,U_R \tag{6}$$

where Φ_R is the $n_R \times n_R$ partition of the full modal matrix Φ containing only the DOF and modes to be retained in the reduced model. M_i, ζ_i, and ω_i are, respectively, the modal masses, inherent damping ratios, and undamped natural frequencies of the retained modes. We will call this reduction method the modal reduction method because it preserves exactly the first n_R modes and frequencies.

The second model reduction scheme used herein is the Guyan reduction,[15] which redistributes the system properties to a subset of the total number of DOF preserving the static behavior of the finite element model.

Reduced Model Correction

It is unusual to have good agreement between analytically predicted and experimentally measured vibration frequencies and modes of complex structures. Since the modes and frequencies are used in the control system design, it is important to correct the analytical model to agree with experimental data. Several methods for model corrections are available. The correction method used herein was first proposed by Baruch and Bar-Itzhak in 1978[16] and then extended to the process described by Baruch in 1982.[17] Experimentally measured frequencies and mode shapes are used as the reference basis for this correction. First, the mode shapes are normalized with respect to the uncorrected reduced mass matrix, so that the normalized ith mode $\hat{\Phi}_i$ is related to the uncorrected reduced mode Φ_{Ri} as

$$\hat{\Phi}_i = \Phi_{Ri}(\Phi_{Ri}^T m_{Ri}\Phi_{Ri})^{-1/2} \tag{7}$$

and then the correction to the mass matrix is

$$\hat{m}_R = m_R - m_R\hat{\Phi}(\hat{\Phi}^T m_R\hat{\Phi})^{-1}(\hat{\Phi}^T m_R\hat{\Phi} - I)(\hat{\Phi}^T m_R\hat{\Phi})^{-1}\hat{\Phi}^T m_R \tag{8}$$

where $\hat{\Phi}$ is the corrected reduced modal matrix. The correction to the stiffness matrix is given in terms of a diagonal matrix of experimental frequencies Ω^2 as

$$\hat{k}_R = k_R - k_R\hat{\Phi}\hat{\Phi}^T\hat{m}_R - \hat{m}_R\hat{\Phi}\hat{\Phi}^T k_R + \hat{m}_R\hat{\Phi}\hat{\Phi}^T k_R\hat{\Phi}\hat{\Phi}^T\hat{m}_R + \hat{m}_R\hat{\Phi}\Omega^2\hat{\Phi}^T m_R \tag{9}$$

The damping matrix is determined from the experimental frequencies, damping ratios, and mode shapes as

$$\hat{m}_R^{-1}\hat{c}_R = \hat{\Phi}_R[\mathrm{diag}(2\zeta_i\omega_i)]_R\hat{\Phi}_R^{-1} \tag{10}$$

Linear Quadratic Control

The standard steady-state, deterministic (i.e., $w_1 = 0$) linear quadratic regulator (LQR) has a performance index of the form

$$J = \int_0^\infty [x(t)^T Q x(t) + u(t)^T R u(t)]\,dt \tag{11}$$

where Q and R are weighting matrices[18] chosen here so as to insure a minimum value ζ_L for the damping ratios of the first n_m modes. The optimum value of the performance index with a given vector x_0 of initial conditions is

$$J_{\min} = x_0^T\,S\,x_0 \tag{12}$$

where S is found by solving an algebraic matrix Riccati equation. The initial conditions chosen for comparison are the first n_f open-loop mode shapes, each normalized with a maximum deflection of 1 in., $x_0^T = [\mathbf{0}, \phi_i^T]$.

Since we cannot measure all of the states and since measurement noise is present, we obtain an estimate $\hat{x}$ to the state with an observer that solves

$$x'(t) = Ax'(t) + Bu(t) + K[y(t) - Cx'(t)] \tag{13}$$

where y is the sensor output vector of n_s noisy measurements, C the observation matrix relating y to x, and K the observer gain matrix to be determined.[18] If a Kalman filter is used as the observer, then the filter gain matrix is found through the solution of another Riccati equation. This Riccati equation depends on the assumed system noise V_1 and measurement noise matrices V_2 and the prescribed stability margin (alpha shift)[10,19] of the filter poles. With this optimal estimate of the state vector, the control equation is

$$u(t) = -Fx'(t) \tag{14}$$

$$F = R^{-1}B^T S \tag{15}$$

The combined system of LQR and Kalman filter is denoted linear quadratic Gaussian (LQG) control. For assessing the loss of performance associated with the use of an observer rather than measuring the entire state vector, we use the quadratic performance index [Eq. (11)]. The LQG control system can be described with an augmented state vector $\bar{x}$ of dimension $4n$,

$$\dot{\bar{x}}(t) = \bar{A}\bar{x}(t) \tag{16}$$

where

$$\bar{A} = \begin{bmatrix} A - BF & BF \\ 0 & A - KC \end{bmatrix} \tag{17}$$

and the augmented state vector is $\bar{x}^T = [x^T, e^T]$, where the state reconstruction error vector of order $2n$ is

$$e(t) = x(t) - x'(t) \tag{18}$$

The optimal value of the performance index Eq. (11) is given as

$$J_{\min} = \bar{x}_0^T \bar{P} \bar{x}_0 \tag{19}$$

where the $4n \times 4n$ matrix $\bar{P}$ is the solution[11,18] of the Lyapunov equation

$$\bar{A}^T \bar{P} + \bar{P}\bar{A} + \bar{Q} = 0 \tag{20}$$

$$\bar{Q} = \begin{bmatrix} Q + F^T R F & -F^T R F \\ -F^T R F & F^T R F \end{bmatrix} \tag{21}$$

We assume that the initial observer state estimate is $\hat{x}_0 = 0$, and, therefore, the augmented initial state is $[x_0^T, x_0^T]$.

To investigate the effect of model reduction, we analyze a full-order model of the structure connected to the controller designed for the reduced model. The combined structure/controller is a linear system of order $2n + 2n_R$,

$$\dot{x}_E(t) = A_E x_E(t) \tag{22}$$

where $x_E^T = [x^T, x_R^{T'}]$ and

$$A_E = \begin{bmatrix} A & -BF_R \\ K_R C & A_R - K_R C_R - B_R F_R \end{bmatrix} \tag{23}$$

where subscript R denotes the reduced form of the corresponding matrix.

The quadratic performance index for the reduced-order control system can be evaluated as

$$J_{\min} = x_{E0}^T P_E x_{E0} \tag{24}$$

where the matrix P_E of order $2n + 2n_R$ is the solution[11,18] of the Lyapunov equation

$$A_E^T P_E + P_E A_E + Q_E = 0 \tag{25}$$

with

$$Q_E = \begin{bmatrix} Q & 0 \\ 0 & F_R^T R F_R \end{bmatrix} \tag{26}$$

We assume that the initial observer state estimate is $x'_{R0} = 0$, and, therefore, the augmented initial state is $x_{E0}^T = [x_0^T, 0]$.

Minimized Maximum Force Direct Rate Feedback Control

Minimized maximum force direct rate feedback control (MFDRF) is a special case of direct output feedback control. Active vibration damping is effected by pairs of collocated velocity sensors and force actuators. The number of control pairs n_c is typically much smaller than the order of x, and only a vector y of n_c velocity elements $\dot{q}_j$ of the state vector is fed back in the closed loop,

$$u(t) = -Dy(t) \tag{27}$$

or

$$u_i = -\sum_{j=1}^{n_c} d_{ij} \dot{q}_j, \qquad i = 1, \ldots, n_c \tag{28}$$

System stability is guaranteed if the active damping matrix D ($n_c \times n_c$) is positive definite because this form of active damping can only dissipate energy.[4,6,12] Therefore, we require D be positive definite as a constraint and, additionally, impose minimum stability margins on selected modes of the structure.

The performance index selected here for obtaining the gain matrix D is the minimization of the maximum actuator force, assuming that each sensor has the same velocity bound. This index is chosen because the required stability margins limit the system response, and so the objective function should minimize the size of the actuators. Assuming that each velocity bound is $\dot{q}_{\max}$, then the maximum possible actuator force $u_{\max}$ for each actuator is proportional to f_i

$$f_i = \frac{u_{\max}}{\dot{q}_{\max}} = \sum_{j=1}^{n_c} |d_{ij}| \qquad i = 1, \ldots, n_c \tag{29}$$

The elements of D are then determined such that the control force ratio f_i for each actuator is less than or equal to a value γ. The variable γ is then minimized subject to constraints. The optimum design problem is formulated as:

find D to minimize γ subject to

$$g_j = \zeta_j - \zeta_L \geq 0 \qquad j = 1, \ldots, n_m \tag{30}$$

D positive definite

and

$$\sum_{j=1}^{n_c} |d_{ij}| \geq \gamma \qquad i = 1, \ldots, n_c$$

where g_j are constraints on the stability of the closed-loop system, expressed as lower limits ζ_L on the damping ratios ζ_j of the first n_m modes. The absolute value function does not have continuous derivatives at zero and is replaced by a quartic polynomial near zero.[11] The minimization problem is solved numerically using the NEWSUMT-A program.[20]

For comparison with the LQG design, the performance index of Eq. (11) is calculated for a direct rate feedback design for a given set of initial conditions x_0 as:

$$J_{\min} = x_0^T \tilde{P} x_0 \tag{31}$$

where $\tilde{P}$ is obtained from the Lyapunov equation

$$\tilde{A}^T \tilde{P} + \tilde{P}\tilde{A} + \tilde{Q} = 0 \tag{32}$$

where

$$\tilde{A} = A - BF_D, \qquad \tilde{Q} = Q + F_D^T R F_D \tag{33}$$

where F_D is the gain matrix containing the elements of D as its only nonzero elements at the DOF where control pairs are located.

Linear Quadratic Direct Rate Feedback Control

A second direct rate feedback control law is the linear quadratic direct rate feedback (LQDRF) law based on the quadratic performance index of the LQ design. The LQ design minimizes the quadratic performance index for all initial conditions. This is impossible to achieve with direct rate feedback. Instead, the LQDRF law minimizes the quadratic performance index for initial conditions in the shape of a number n_f of natural vibration modes. That is,

$$J_{\text{LQDRF}} = \max_{i=1,\ldots,n_f} J_i / J_{i0} \tag{34}$$

where

$$J_i = \int_0^\infty \left[x(t)^T Q x(t) + u(t)^T R u(t) \right] \mathrm{d}t$$

for

$$x_0 = [0^T, \phi_i^T]^T$$

where J_{i0} is a normalization parameter. As with the other two control laws, lower limits ζ_L on the damping ratios ζ_i of the first n_m modes are also imposed. Because the maximum function in Eq. (34) can have discontinuous derivatives, an equivalent formulation is used for the design as follows:

find β and the elements of D to minimize β

such that $$J_i / J_{i0} \leq \beta \quad i = 1, \ldots, n_f \tag{35}$$

$$g_j = \zeta_j - \zeta_L \geq 0 \quad j = 1, \ldots, n_m$$

and D positive definite

The Q and R matrices here are the same as in the LQ design. The quadratic performance index is calculated as in Eqs. (31-33). This optimization problem is also solved by NEWSUMT-A.[20]

Laboratory Grid Structure

The control laws described in the previous sections have been applied to a small laboratory grid structure illustrated in Fig. 1. The major components are a lightweight skewed grid of aluminum beams, two nominally identical thick aluminum plates, and a steel top beam assembly from which the grid and the plates hang vertically. All members of the structure are bolted tightly together at the joints, 12 of which are labeled on Fig. 1. The structure has both out-of-plane and in-plane vibration modes relative to the grid plane, but the two types of modes are decoupled by the geometry. Only out-of-plane excitation and response are considered herein, and so all subsequent discussion refers to out-of-plane dynamics.

The structure is modeled with 30 beam finite elements connected at 22 grid points, numbered on Fig. 1. The DOF at each grid point are out-of-plane translation and rotations about the horizontal and vertical in-plane axes. Translations are restrained at grid points 13 and 22 and so the total number of DOF is 64.

The beam element stiffness and mass matrices used for the aluminum grid are standard, with bending deformation based on Euler-Bernoulli theory and cubic shape functions and torsional deformation based on linear shape functions.[21] One exception of this standard approach is that bending shear flexibility is included to account at least roughly for the discontinuous sandwich design of the top beam evident in the top view of Fig. 1. Gravity-induced in-plane axial forces, shear forces, and bending moments have significant influence on the out-of-plane stiffnesses of the thin-walled aluminum grid members. This influence is represented by element geometric stiffness matrices.[22]

The thick aluminum plates are modeled as being rigid. The product of weight W times eccentricity Y of each plate acts as a pendulous rotational stiffness about the beam assembly axis at the location where the plate joins the beam assembly. This is modeled by the attachment of a grounded rotational spring with stiffness WY at grid points 13 and 22.

Inherent damping equivalent to the measured open-loop damping for the first 12 modes was included in the analysis along with a nominal level of 1% damping in the higher modes. The measured frequencies are in generally good agreement with the analytical frequencies, see Table 1. Because of control hardware limitations, the size of the model must be reduced so that the controls may be implemented. The modes with frequencies under 10 Hz are of primary interest. Therefore, we retain the 12 modes under 10 Hz in our reduced model.

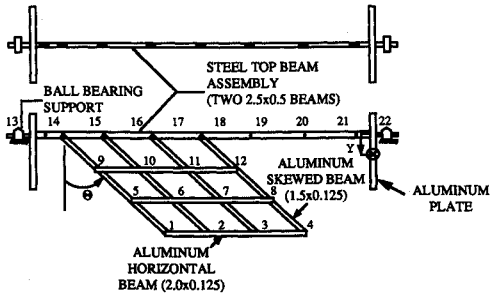

Fig. 1 Line drawing of the laboratory structure with grid points numbered: $\theta = 45$ deg; $Y = 9.05$ in.

Correction of Reduced Models

For the modal reduction method, we kept the 12 translations at the joints on the aluminum grid since they have the largest displacements. For the Guyan reduction, minimum degradation of accuracy was obtained by keeping the displacements at joints 1-9 and 12 on the aluminum grid and the rotations at the ball bearing supports of the top beam. When we compared the analytical open-loop behavior of the reduced models with experimental results, we found that the mode shapes were inaccurate enough to cause degradation of the performance of the control systems. Therefore, we attempted to correct both of the reduced models with the experimental modes and frequencies.

To determine whether the correction process really works, it was applied in a sequential manner one mode at a time. The correction process was deemed successful if the correction of the lower frequencies and modes also improved the accuracy of the higher frequencies. For the modal reduction model, this correction process did not work, with large errors introduced in the higher frequencies upon correction of the lower ones. The Guyan reduction model, on the other hand, responded well to the correction process. Eleven experimental modes were used and the correction reduced the error in the 12th frequency from 18 to 0.5%.

In the following, the modal reduction model is used as the uncorrected model because it is in much better agreement with the experimental results than the Guyan reduction model. The corrected Guyan reduction model is used as the corrected model because of its amenability to the correction process. The following section compares the control systems for these two models.

Comparison of Control Systems—Analytical Results

The control system includes five force actuators (to be described later),[23] each collocated with a velocity sensor (i.e., $n_c = n_s = 3$) at joints 1, 2, 4, 5, and 8. Analytical results from controllers that were designed based on the uncorrected (modal reduction) model are presented first and the results from the corrected Guyan reduced model later in this section. Because the aim of the direct rate feedback control system is to achieve simplicity and robustness, a simplified LQDRF design was also considered. The design is limited to a diagonal matrix D so that the control actuators are uncoupled, with each sensor/actuator pair constituting, in effect, an electric dashpot. We found that the limitation to a diagonal D did not affect performance adversely, and so only this design is considered in the following.

The LQR control system was designed with $Q = 0.01I$ and $R = 0.84I$, selected to achieve a minimum of 3% damping in the first five (n_m) vibration modes. The direct rate feedback controllers were designed with the same stability margins. The LQDRF design used the same Q and R matrices, and the normalization parameter J_{i0} was selected to be 1. Two normalization strategies were used for the LQDRF control. Initial

Table 1 Open-loop frequencies

Mode number	Finite element model, Hz	Experiment, Hz
1	0.593	0.687
2	0.840	0.969
3	1.45	1.47
4	3.35	3.33
5	3.60	3.64
6	5.14	5.22
7	5.57	5.57
8	5.75	5.78
9	6.22	6.34
10	8.08	7.89
11	8.50	8.39
12	9.60	9.60

conditions in the form of the first $n_f = 5$ mode shapes were used for the minimization routine.

Table 2 displays the two direct rate feedback designs (i.e., matrix D) produced. The gains in the LQDRF design are generally larger than the gains for the MFDRF design, and it is seen that the MFDRF design has very small off-diagonal terms.

The Kalman filter was designed for the LQG control system with alpha shift ($\alpha = 0.05$) and noise matrices ($V_1 = 10^{-10}I$, $V_2 = 0.5I$) selected to make the real parts of the filter poles about three times larger than the real parts of the regulator poles. The alpha shift dominated the design, whereas the noise matrices had an insignificant influence.

Table 3 contains the damping ratios for the two DRF designs as well as for the LQG controller that was designed with the reduced model applied to both the reduced model and the full model [obtained from the eigenvalues of A_E, Eq. (23)]. Comparing the two LQG columns, it is seen for the first five controlled modes that the model reduction and the Kalman filter have little effect on the damping ratios. Applying the DRF control laws that were designed with the reduced model to the full model produced only minor differences in the third significant figure of the damping ratios and performance indices.

Quadratic performance indices (using $Q = 0.01I$, $R = 0.84I$) were calculated [see Eqs. (19) and (24)] for initial conditions in the form of the first five open-loop mode shapes; results are presented in Table 4.

Comparison of the LQR and LQG columns shows that the deterioration in performance due to the need for an observer is significant in all modes. Model reduction effects on the performance indices are minimal as is displayed by the small increases in the indices when the reduced model controller is applied to the full model. The reduced model LQG design applied to the full model performs better than the DRF designs for the first two modes and not as well in modes 3-5. For higher modes not included in the LQDRF design (and not shown in Table 4), the LQG design was generally better. Comparison of the two direct rate feedback laws shows that the LQDRF design was generally better than MFDRF, which is expected since MFDRF has a different design objective. Overall, the loss of performance due to model reduction and state reconstruction for LQG control balances the loss due to the LQDRF design being suboptimal. Spillover effects from applying a controller design with a reduced model to the full model were present in three of the modes not included in the reduced mode. We assumed that these modes had 1% damping in the open-loop model, and when the reduced model LQG controller was applied to the full model, the damping for modes 25, 26, and 33 was reduced below this 1%. The direct rate feedback control laws increased the damping in all modes up to number 45 and did not affect the rest of the modes.

Controllers designed with the corrected Guyan reduced model were similar to the controllers just described with some significant differences. The MFDRF controller again is primarily a diagonal matrix but all of the diagonal terms are nonzero and their values are about half of the previous design. This design uses about 40% less control force than the first MFDRF design. LQR control required $Q = 0.01I$ and $R = 1.387I$ to produce a minimum of damping ratio of 0.03 in the first five modes. Table 5 contains the damping ratios that these new controller designs produced. Comparing these damping ratios with the damping ratios in Table 3, it is evident that the new controllers produce significantly different results. Performance indices (not tabulated) displayed the same trends for this model as they did for the previous model. The DRF designs were better in the higher design modes and LQG control was better in the lowest modes.

To determine the effects the form of the Q matrix has on the performance of the controlled system, we selected a different Q matrix and calculated LQR, LQG, and diagonal LQDRF controllers. The Q matrix selected was

$$Q = \begin{bmatrix} M & 0 \\ 0 & K \end{bmatrix} \tag{36}$$

where $\frac{1}{2}x^T Q x$ represents the total energy of the structure. The R matrix needed to produce a minimum damping ratio of 0.03 in the first five modes was $R = 7.5 \times 10^5 I$. The same noise covariance matrices were used to calculate the Kalman filter for LQG control as before. The performance indices that resulted from these calculations displayed the same behavior that was noted earlier.

Table 2 Gain matrices D for DRF control (lb-s/in.)—uncorrected model (modal reduction)[a]

Actuator joint number	MFDRF control sensor joint number				
	1	2	4	5	8
1	0.0050	0.0001	0.0000	−0.0001	−0.0001
2	0.0001	0.0060	0.0000	−0.0001	0.0000
4	0.0000	0.0000	0.0000	0.0000	0.0000
5	−0.0001	−0.0001	0.0000	0.0055	0.0001
8	−0.0001	0.0000	0.0000	0.0001	0.0058

[a]Diagonal LQDRF control diag (0.0062, 0.0058, 0.0096, 0.0057, 0.0061).

Table 3 Closed-loop damping ratios from reduced model designs—uncorrected model (modal reduction)

Mode number	LQG	LQG applied to full-model	MFDRF	Diagonal LQDRF
1	0.1177	0.1176	0.1272	0.3094
2	0.5315	0.5298	0.0518	0.1275
3	0.2318	0.2317	0.1045	0.1435
4	0.0514	0.0514	0.0325	0.0742
5	0.0299	0.0300	0.0300	0.0301

Experimental Apparatus and Procedure

Experiments were conducted to test the accuracy of the theoretical predictions against laboratory measurements of the control system performance. The direct rate feedback control schemes and the LQG design described in the previous sections were tested on the structure using identical control hardware. Velocity frequency response functions (VFRFs) were measured at several joints on the grid and compared with analytical VFRFs for the same locations. The basic experimental appara-

Table 4 Quadratic performance index ($Q = 0.01I$, $R = 0.84I$) —uncorrected model (modal reduction)

Initial conditions mode number	Full-model controller		Reduced model applied to full model	Reduced model controllers			
	LQR	LQG	LQG	LQR	LQG	MFDRF	LQDRF
1	0.617	0.766	0.778	0.622	0.777	1.629	0.956
2	0.553	0.586	0.589	0.554	0.588	1.603	0.779
3	0.682	1.011	1.012	0.685	1.011	0.948	0.787
4	1.077	1.427	1.431	1.073	1.427	1.441	1.284
5	3.926	4.558	4.570	3.908	4.550	4.007	3.924

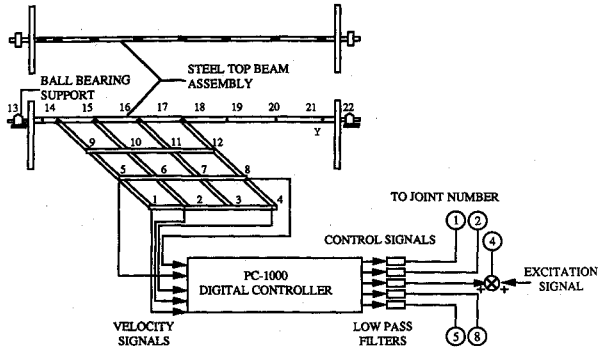

Fig. 2 Schematic diagram of the control system.

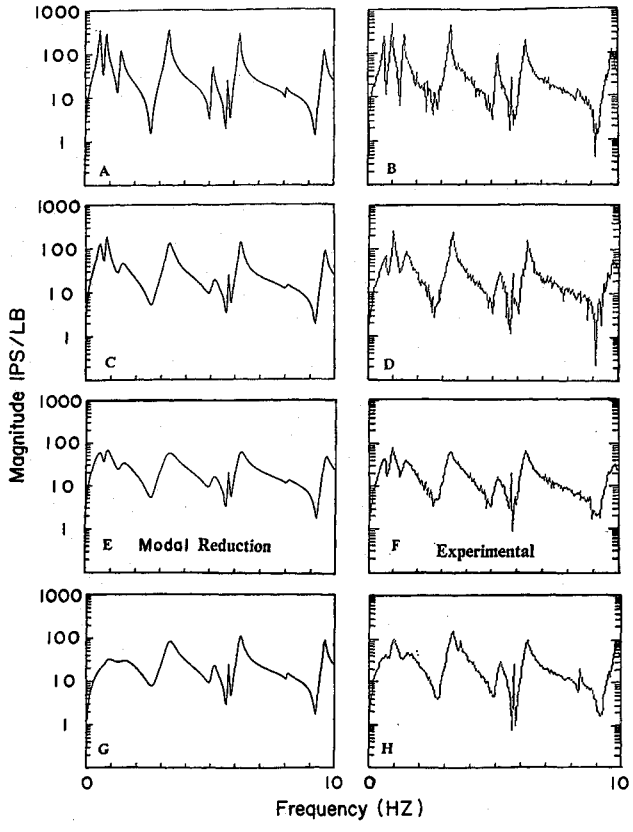

Fig. 3 Experimental and theoretical velocity-to-force frequency response function of response at grid point 4 (modal reduction): a) and b) open-loop system; c) and d) MF-DRF design; e) and f) diagonal LQ-DRF design; g) and h) LQG.

tus and procedures are described in detail in Refs. 6 and 23. A summary of the apparatus used and the procedure relevant to this paper is provided here.

Each noncontracting velocity sensor and force actuator consisted of a small structure-borne coil moving within an annular magnetic field generated by an externally supported magnetic field assembly. Movement of a velocity sensing coil through the magnetic field produced a voltage proportional to the velocity, and application of a current to a force actuator coil produced a proportional control force. Figure 2 is a schematic diagram of the structure and control system. Each velocity sensor voltage was first fed into a very high input impedance operational amplifier and passed to the digital controller.

The PC-1000 digital controller built by Systolic Systems, Inc., processed the signals according to the control law being tested. The PC-1000 is a small desktop unit operated through a host IBM-PC personal computer. It has 16 channels available for input from sensors, a high-speed array processor for

Table 5 Closed-loop damping ratios from corrected Guyan model designs

Mode number	LQG	MFDRF	Diagonal LQDRF
1	0.3572	0.0822	0.0979
2	0.0741	0.0300	0.0335
3	0.1582	0.0575	0.0704
4	0.3917	0.0332	0.0389
5	0.0300	0.0300	0.0309

Table 6 Analytical/experimental peak level ratios

Mode number	Open loop		LQG		MFDRF		LQDRF	
	UM[a]	CG[b]	UM	CG	UM	CG	UM	CG
1	1.78	1.25	0.47	0.99	2.02	1.42	1.41	1.23
2	0.86	0.72	0.35	1.09	0.75	1.32	0.92	1.10
3	0.55	1.02	0.65	0.59	0.55	0.75	0.85	0.99
4	0.98	1.38	0.55	0.66	0.55	0.54	0.94	0.90
Average	0.35	0.23	0.49	0.22	0.54	0.36	0.18	0.11

[a]UM-Uncorrected modal. [b]CG-Corrected Guyan.

doing calculations with the digitized sensor signals, and 16 channels for output signals to drive control actuators. The PC-1000 has a sampling rate variable from 2 to 2000 samples/s, and for the present study the control laws were implemented at a sampling rate of 2000/s. When operated at high sampling rates with structural frequencies under about 20 Hz, the PC-1000 appears, for most practical purposes, to be a continuous time (analog) instrument rather than a discrete time (digital) instrument since the phase lag produced by digital data acquisition and processing is very small. The actual time delay through the PC-1000 was found to be $1.3\Delta t$, where Δt is the sampling period.

The control signals generated by the PC-1000 were filtered by single-stage passive RC low-pass filters (corner frequency, 200 Hz). These filters were primarily smoothing filters present to eliminate the stair-step nature of the output signals from the PC-1000's zero-order hold digital-to-analog converter. Each control signal finally passed into a controlled-current power amplifier, which produced a current proportional to the input voltage to drive the actuator.

An STI-11/23 data acquisition and analysis system developed by Synergistic Technology, Inc., generated excitation signals, received measurement sensor signals, and performed all data analysis. The excitation signal was added to the control feedback signal for grid point 4, so that one actuator served the dual purpose of control actuator and exciter.

Velocities were measured at joints 1-5 and 8 on the grid. Force input to the structure was measured at joint 4. The velocities at joints 1, 2, 4, 5, and 8 were used in the controller. Random excitation was used to force the structure. To achieve a good signal-to-noise ratio, the general excitation level was set as high as possible consistent with maintaining linear behavior of the velocity sensors and force actuators. Fast Fourier transforms of the response and excitation signals were calculated and the former was divided by the latter to produce a VFRF. The frequency resolution was 0.0391 Hz. In all cases, the VFRFs calculated from a single excitation period without data windowing were reasonably smooth and repeatable, so that neither averaging nor windowing of the experimental data was necessary.

Comparison of Analytical and Experimental Results

Representative VFRF magnitudes are presented in Figs. 3 for the analytical and experimental open-loop system (Figs. 3a and 3b), MFDRF (Figs. 3c and 3d), LQDRF (Figs. 3e and 3f), and LQG (Figs. 3g and 3h) controllers designed from the uncorrected (modal reduction) model. Figures 4 are the same matrix of plots for the corrected Guyan reduced designs. The open-loop analytical results and measurements verify the

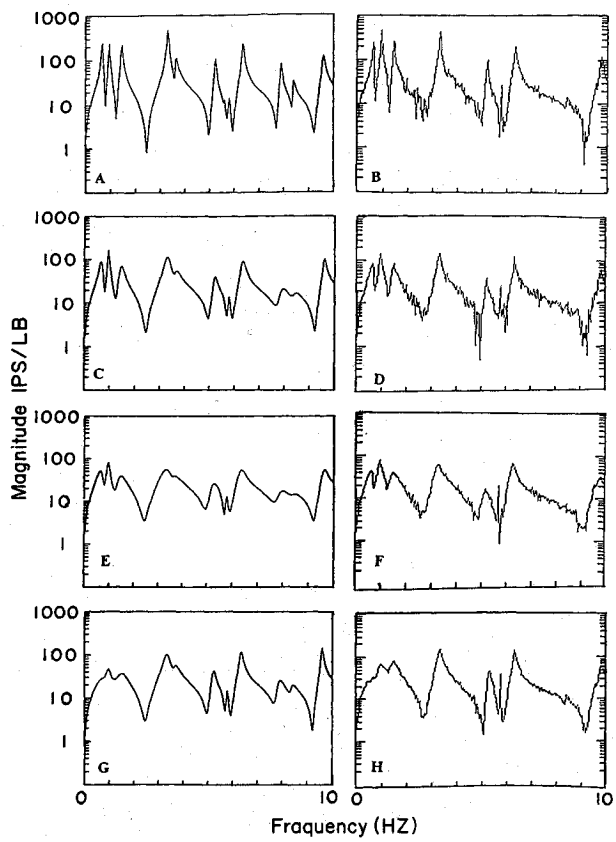

Fig. 4 Experimental and theoretical velocity-to-force frequency response function of response at grid point 4 (corrected reduction): a) and b) open-loop system; c) and d) MF-DRF design; e) and f) diagonal LQ-DRF design; g) and h) LQG.

structural model, in general, but a close look at the relative heights of the peaks reveals some discrepancies. Table 6 lists the ratios of the analytic peak levels to the experimental peak levels for the open-loop system and the three controlled systems. There are two columns in each category. These are the ratios for the uncorrected model and the corrected Guyan reduced model. Four modes are listed for each system followed by a summary row, which is the average of the absolute value of 1 minus the ratio. The discrepancies in the peak levels are due to modeling errors.

For the open-loop system, the ratio for the uncorrected model is better in modes 2 and 4 and the corrected Guyan model is better in modes 1 and 3. The summary row reveals that the corrected Guyan reduced model has better overall agreement than the uncorrected model. Comparing Figs. 3a and 3b with Figs. 4a and 4b shows that the corrected Guyan model has a better overall VFRF shape match up to 7 Hz and from then on the uncorrected model is a better match.

The closed-loop VFRFs exhibit many of the same characteristics as the open-loop VFRFs with some differences. For the LQG controller (Figs. 3g, 3h, 4g, and 4h), both the uncorrected model and the corrected Guyan model predict lower response levels than actually occur (Table 6 ratios are smaller than 1), whereas the open-loop VFRFs are both higher and lower depending on the mode. The summary row in Table 6 again shows that the corrected Guyan model has more accurate peak levels than the uncorrected model. With MFDRF control (Figs. 3c, 3d, 4c, and 4e) applied to the structure, the analytic VFRF predictions are this time both high and low with respect to the experimental peak levels. The average difference for MFDRF control on the uncorrected model (54%) is the worst of any of the comparisons, and diagonal LQDRF control on the corrected Guyan model (11%) has the best comparison. LQDRF control (Figs. 3e, 3f, 4e, and 4f) has the best agreement between experiment and theory of any of the control systems tested. Overall, it appears that the corrected model has better agreement with the experiments than the uncorrected one and that the best agreement is attained for the simplest control—the diagonal LQDRF.

Concluding Remarks

An analytical and experimental investigation of active vibration damping of a laboratory grid structure was presented. Two reduced structural models and three control laws were used to design the control system. One reduced model preserves the lowest frequencies and model shapes, but did not lend itself to correction based on experimentally measured normal modes and frequencies. The other model, based on the Guyan reduction, is less accurate but lends itself better to correction based on experimental measurements. The three control laws considered included a time-invariant linear quadratic regulator with state estimation and two direct rate feedback control laws. All three were found to have comparable performance based on analytical simulations. Experimental verification of the open- and closed-loop systems showed that for all of the systems investigated the corrected Guyan reduced model predicted the peak levels better than the uncorrected model. Also, the best analytical-experimental correlation was obtained for the simplest control law—an uncoupled direct rate feedback control.

Acknowledgments

The research reported in this paper was supported in part by NASA Grant NAG-1-224, contract monitor H. M. Adelman. W. L. Hallauer's consultation and recommendations greatly aided the experimental portion of this research.

References

[1]Balas, M. J., "Trends in Large Space Structures Control Theory: Fondest Hopes, Wildest Dreams," *IEEE Transactions on Automatic Control,* Vol. AC-27, No. 3, 1982, pp. 522–535.

[2]McLaren, M. D., and Slater, G. L., "Robust Multivariable Control of Large Space Structures Using Positivity," *Journal of Guidance, Control, and Dynamics,* Vol. 10, No. 4, 1987, pp. 393–400.

[3]Martinovic, Z. N., Schamel, G. C., Haftka, R. T., and Hallauer, W. L., Jr., "Analytical and Experimental Investigation of Output Feedback vs. Linear Quadratic Regulator," *Journal of Guidance, Control, and Dynamics,* Vol. 13, No. 1, 1990, pp. 160–167.

[4]Joshi, S. M., "Robustness Properties of Collocated Controllers for Flexible Spacecraft," *Journal of Guidance, Control, and Dynamics,* Vol. 9, No. 1, 1986, pp. 85–91.

[5]Haftka, R. T., Martinovic, Z. N., Hallauer, W. L., Jr., and Schamel, G. C., "Analytical and Experimental Study of Control System Sensitivity to Structural Modifications," *AIAA Journal*, Vol. 25, No. 2, 1987, pp. 310–315.

[6]Skidmore, G. R., and Hallauer, W. L., Jr., "Experimental-Theoretical Study of Active Damping With Dual Sensors and Actuators," AIAA Paper 85-1921, Aug. 1985.

[7]Juang, J.-N., and Horta, L. G., "Effects of Atmosphere on Slewing Control of a Flexible Structure," *Journal of Guidance, Control, and Dynamics,* Vol. 10, No. 4, 1987, pp. 387–392.

[8]Martinovic, Z. N., Haftka, R. T., Hallauer, W. L., Jr., and Schamel, G. C., II, "A Comparison of Active Vibration Control Techniques: Output Feedback vs. Optimal Control," AIAA Paper 87-0904, April 1987.

[9]Hallauer, W. L., and Barthelemy, J. F. M., "Active Damping of Modal Vibrations by Force Apportioning," AIAA Paper 80-0806, May 1980.

[10]Kammer, D. C., and Sesak, J. R., "Actuator Number Versus Parameter Sensitivity in Flexible Spacecraft Control," *Proceedings of Second VPI & SU/AIAA Symposium on Dynamics and Control of Large Flexible Spacecraft,* edited by L. Meirovitch, Blacksburg, VA, 1979, pp. 421–441.

[11]Martinovic, Z. N., "Sensitivity of Active Vibration Control to Structural Changes and Model Reduction," Ph.D. Dissertation, Virginia Polytechnic Inst. and State Univ., Blacksburg, VA, May 1987.

[12]Canavin, J. R., "The Control of Spacecraft Vibrations Using Multivariable Output Feedback," AIAA Paper 78-1419, Aug. 1978.

[13]Haftka, R. T., Martinovic, Z. N., and Hallauer, W. L., Jr., "Enhanced Vibration Controllability by Minor Structural Modification," *AIAA Journal*, Vol. 23, No. 8, 1985, pp. 1260–1266.

[14]Sparks, D. W., Jr., Juang, J-N., and Klose, G. J., "A Survey of Experiments and Experimental Facilities for Control of Flexible Structures," *Proceedings of AIAA Guidance, Navigation and Control Conference*, AIAA, Washington, DC, Aug. 1989, pp. 1176–1185.

[15]Guyan, R. J., "Reduction of Stiffness and Mass Matrices," *AIAA Journal*, Vol. 3, No. 2, 1965, p. 380.

[16]Baruch, M., and Bar-Itzhak, I. Y., "Optimal Weighted Orthogonalization of Measured Modes," *AIAA Journal*, Vol. 16, No. 4, 1978, pp. 346–351.

[17]Baruch, M., "Optimal Correction of Mass and Stiffness Matrices Using Measured Modes," *AIAA Journal*, Vol. 20, No. 11, 1982, pp. 1623–1626.

[18]Kwakernaak, H., and Sivan, R., *Linear Optimal Control Systems*, Wiley, New York, 1972.

[19]Anderson, B. D. O., and Moore, J. B., *Linear Optimal Control*, Prentice-Hall, Englewood Cliffs, NJ, 1971, p. 50.

[20]Thareja, R., and Haftka, R. T., "NEWSUMT-A, A General Purpose Program for Constrained Optimization Using Constraint Approximations," *Journal of Mechanics, Transmission, and Automation in Design*, March 1985, pp. 94–99.

[21]Craig, R. R., Jr., *Structural Dynamics, An Introduction to Computer Methods*, Wiley, New York, 1981, pp. 383–389.

[22]Argyris, J. H., Hilpert, O., Malejannekis, G. A., and Scharpf, D. W., "On the Geometrical Stiffness of a Beam in Space—A Consistent V. W. Approach," *Computer Methods in Applied Mechanics and Engineering*, Vol. 20, 1979, pp. 105–131.

[23]Skidmore, G. R., "Experimental Theoretical Study of Velocity Feedback Damping of Structural Vibrations," Ph.D. Dissertation, Virginia Polytechnic Inst. and State Univ., Blacksburg, VA, May 1985.